AN EXAMINATION OF HELICOPTER ROTOR LOAD CALCULATIONS

Thomas H. Maier
U.S. Army Aeroflightdynamics Directorate
Moffett Field, California

ABSTRACT

The structural response of three full-scale helicopter rotors has been examined. Airloads predicted by CAMRAD were compared by harmonics with test measurements. Flapwise bending moments were calculated from the CAMRAD airloads using three methods: force integration, curvature, and a finite-difference method. The force-integration and curvature moments were calculated with the CAMRAD program itself; however, the finite-difference method was calculated externally by a forced response program, Blade Response to Aerodynamic Loading (BRAL). The BRAL analysis with measured airloads was shown to agree well with strain-gauge measurements on the CH-34 rotor in a wind tunnel. The CAMRAD/force-integration bending moments were shown to accumulate error as the integration progressed from tip to root. The CAMRAD/curvature moments agreed well with the finite-difference moments over most of the blade; however, at regions of rapidly changing stiffness the agreement was poor. When applied to the BRAL solution, force integration was shown to give excellent results, provided the integration had a small step size. Shear forces calculated by CAMRAD and BRAL showed fair agreement.

INTRODUCTION

The calculation of helicopter rotor-blade bending moments is aeroelastic in nature. Aerodynamic, inertial, and elastic forces must balance to provide equilibrium of the rotor blade. Although the bending moments are embedded in the equilibrium solution, they are typically calculated separately after the equilibrium solution has been obtained. There are two common ways of doing this. The bending moments are either calculated as the integral of the aerodynamic and inertial forces or they are calculated as the product of stiffness and curvature.

The relative merits of these two methods have been examined in the literature.[1–4] All have concluded that force integration is more accurate and that it converges with fewer modes. Bielawa[3] pointed out that the increased accuracy of force integration is paid for by increased complexity and that force integration requires greater attention to details of its implementation. Numerical problems arise for both methods. The curvature method requires the calculation of the second derivative of the deflected shape, and the force-integration method requires that the difference of large forces be integrated along the blade span. If the structure has rapid changes in stiffness and mass, there must also be rapid changes in the deflected shape. This requires many modes with a modal analysis or many elements with a finite-element analysis. This also requires that the force-integration method have small enough intervals to accurately evaluate the deflections and the spanwise distribution of structural properties.

Hodges[4] developed the direct method of Ritz as a finite-element method and demonstrated that it could achieve the "exact" solution when elements spanned regions of analytic stiffness and mass. He compared this with conventional applications of the Rayleigh-Ritz method in which both force integration and curvature were used to calculate bending moments. He concluded that the force-integration method was more accurate than the curvature method but that the Ritz finite-element method was superior to both.

In correlating results from a Comprehensive Analytical Model of Rotorcraft Aerodynamics and Dynamics, CAMRAD, with flight test data for the SA349/2 rotor it was reported that the calculated flapwise bending moments were sensitive to the blade-mass distribution.[5] At that time CAMRAD calculated bending moments using the force-integration method. CAMRAD was changed, however, to calculate bending moments using the curvature method; the

[1]Presented at the American Helicopter Society National Specialists' Meeting on Rotorcraft Dynamics, Arlington, Texas, November 1989.

result was a significant improvement in loads correlation.[5] Subsequent loads-correlation efforts using CAMRAD have relied on the curvature method.[6,7] The superiority of the curvature method in CAMRAD is surprising considering the conclusions of Refs. 1-4.

This paper examines the calculation of flapwise bending moments after an equilibrium solution has been obtained. CAMRAD is used to obtain the aeroelastic equilibrium solution for three full-scale rotors: the CH-34, SA349/2, and BO-105. Subsequent flapwise bending moment calculations will be made with CAMRAD using both the force-integration and curvature methods. The airloads from the CAMRAD equilibrium solution are also used as the forcing function for an independent finite-difference response analysis that is used to evaluate results of the two methods calculated in CAMRAD. The finite-difference solution is used to make general conclusions about the force-integration and curvature methods for calculating bending moments for realistic full-scale helicopter rotors.

CAMRAD CALCULATION

CAMRAD is used to calculate trim, airloads, blade deflections, and structural loads. A detailed description of the theoretical basis of CAMRAD is given in Ref. 8. The blade structural analysis follows the work of Houbolt and Brooks[9] with important nonlinear effects included in the inertial and aerodynamic forces. The aerodynamic model is based on lifting-line theory, using steady two-dimensional airfoil characteristics and a vortex wake. Blade aerodynamic and structural models provide the section forces. Equilibrium of inertial, aerodynamic, and elastic forces determines the differential equations of motion. The blade degrees of freedom are flap/lag bending, rigid pitch, and elastic torsion modes.

Once CAMRAD has calculated the trim, airloads, and blade deflections, the bending moments are calculated. The original version of CAMRAD documented in Ref. 8 calculates the bending moments using the force-integration method. As mentioned in the introduction, a modification was written to CAMRAD which calculates bending moments using the curvature method. Results from both methods will be shown.

Additional modification to the CAMRAD analysis used here has improved the high-speed flight airload calculation.[10] An improved wake model has been incorporated in the analysis. It includes a dual-peak circulation model, to more accurately model the negative loading at the tip on the advancing side of the disk, and second-order lifting-line theory, to better model blade-vortex interaction. This is essentially the aerodynamic model available in CAMRAD/JA.[11]

FINITE-DIFFERENCE STRUCTURAL RESPONSE ANALYSIS

To aid in the comparison of the two bending-moment calculations implemented in CAMRAD a fine-resolution, finite-difference structural response analysis has also been used. The Blade Response to Aerodynamic Loading (BRAL) program originated from the work of Esculier and Bousman.[12] BRAL calculates the coupled flap/lag/torsion structural response of the helicopter rotor to given aerodynamic loading as described in Ref. 12. A periodic solution is assumed in the time domain and is represented by Fourier harmonic functions. The linear Houbolt and Brooks[9] equations of motion are solved for each harmonic as a two-point boundary value problem. In effect, this is a finite-difference method with several hundred spanwise grid points. The BRAL analysis has been validated using airloads measured on the CH-34 in a wind tunnel.[13]

These measured airloads were used as the forcing functions to calculate bending moments using BRAL with 400 spanwise intervals. Figure 1 compares the BRAL flap-bending moment with wind-tunnel measurements. This figure shows the flap-bending moment time-history at 45% blade span in the upper left-hand corner. Following the time-history are spanwise distributions of the steady and first six harmonics of the flap-bending moment. The amplitude scale of the harmonic components was allowed to vary so that the spanwise shape of the components could be seen. Although BRAL uses a linear structural model, the resulting correlation is excellent.

In-vacuum blade modes were calculated to ensure that the structural models were as similar as possible. CAMRAD modes were calculated using the flutter analysis option, and BRAL modes were calculated by a companion program, Coupled Modes (CMODES). CMODES calculates the roots to the homogeneous form of the equations of motion found in BRAL, using the frequency determinant.[14] Frequency diagrams for the CH-34, SA349/2, and BO-105 rotors are shown as Figs. 2, 3, and 4, respectively. Agreement is excellent for the CH-34 rotor and fair for the others. The greatest disagreement occurs for the first torsion frequency. The CMODES program does not include steady deformation caused by center of gravity and tension-center offsets from the elastic axis. When these offsets are set to

zero or when zero bending degrees of freedom are used for the mean deflected shape in CAMRAD, the torsion frequencies show much better correlation.

ROTOR AIRLOAD CALCULATIONS

As described earlier, the calculation of bending moments begins with the aeroelastic equilibrium solution. Normal airloads calculated by the CAMRAD equilibrium solution are presented in this section with test measurements, where available. It is important to note that the CAMRAD airloads are identical for each of the BRAL, CAMRAD/force-integration and CAMRAD/curvature-moment results. Although not shown, chordwise airloads and pitching moments are common to these structural moment calculations as well.

Figures 5-7 show the blade normal airloads calculated by CAMRAD and measured in tests, with the exception of the BO-105, for which no test data are available. The CH-34 and SA349/2 rotors are shown at a similar high-speed flight condition; the BO-105 is at a lower speed. Wind-tunnel test measurements of the CH-34 agree very well with the steady component of CAMRAD airloads. Agreement is fair for the first and second harmonic components, but harmonics components above the second harmonic show less agreement. The correlation between the SA349/2 flight-test measurements and CAMRAD airloads is similar to the CH-34 results, although with only three spanwise measurements, conclusions are limited. A distinctive similarity may be seen in the CAMRAD predicted normal airloads for all three rotors.

DEFLECTED SHAPES

The equivalence of the structural models of BRAL and CAMRAD may be seen (Figs. 8-10) by comparing deflected shapes. CAMRAD has iterated to calculate the aeroelastically trimmed solution, and BRAL has calculated the structural response to the CAMRAD airloads. The deflected shapes would be the same for identical structural models, since the airloads are identical. Therefore, differences seen here reflect differences in the structural models.

Figures 8-10 show the flapwise deflected shapes calculated by BRAL and CAMRAD for the CAMRAD airloads just shown. The results are very similar for the three rotors. Disagreement between the two analyses is greatest at the first, third, and fifth harmonics, which are close to the first, second, and third flap modes. This is particularly noticeable for the first harmonic cosine component of the flap deflection for the SA349/2. The proximity of the flap modes to the rotor harmonics is determined by the structural model. It was seen in Figs. 2-4 that the BRAL (CMODES) and CAMRAD modes are not identical. Therefore, the disagreement in deflected shapes may be due to small differences in the modal frequencies.

BENDING MOMENTS

Figures 11-13 show the resulting flapwise bending moments. Test measurements are shown with BRAL, CAMRAD/curvature, and CAMRAD/ force-integration calculations. The time-history plot of Fig. 11 shows CAMRAD/curvature and BRAL predictions agreeing well with one another. The time-history plots of Figs. 12 and 13 show fair agreement between the flight-test measurements, BRAL, and CAMRAD/curvature. The CAMRAD/force-integration results show poor correlation for all three rotors.

Examination of the harmonic components of Figs. 11-13 reveals two consistent discrepancies. First, the CAMRAD/force-integration has the correct zero-moment boundary condition at the tip of the blade, but it appears to accumulate error as forces are integrated toward the root. This is most obvious for the zero-moment boundary condition at the flap hinge of the CH-34 rotor (Fig. 11). This would also be true for the SA349/2, but the BRAL calculation stops at the outboard lag hinge, enforcing the inboard flap hinge boundary condition assuming rigid body motion.

The second discrepancy seen in Figs. 11-13 is the large changes in bending moment predicted by the CAMRAD/curvature method at the root end of the blades. This is caused by large changes in bending stiffness that occur at the root of all three blades (Fig. 14). Seven flapwise bending modes, as used here, are not enough to capture the rapid changes in curvature required to give a smooth product of curvature and stiffness. The phenomenon also appears near the tip of the SA349/2 rotor blade (best illustrated by the first harmonic plot, Fig. 12). In general, it is seen for all three rotors that the results of the CAMRAD/curvature method agree well with those of BRAL away from rapid changes in bending stiffness.

DISCUSSION

Using identical airloads, differences have been shown in the bending moments calculated by the BRAL, CAMRAD/force-integration, and CAMRAD/curvature methods. To the degree that the deflected shapes are similar, these differences are attributed to implementation problems with the force-integration and curvature methods. Depending on the radial station selected, either method will show major errors. Figure 15 demonstrates the severity of the problem near the blade root for both methods.

Insight can be gained by calculating bending moments directly from the BRAL solution. Thus the state-vector (deflection, slope, bending moment, and shear) solution at 300 spanwise intervals was used to calculate the bending moments by the force-integration and curvature methods. Resulting bending moments may be compared with the bending moment of the state vector. The state vector was calculated using the uncoupled flap equation in BRAL for an untwisted CH-34 rotor with the CAMRAD airloads shown in Fig. 5. Inertial forces were calculated from the state-vector deflected shape assuming simple harmonic motion; aerodynamic forces were taken from the CAMRAD solution; and the curvature was calculated as the derivative of the state-vector slope. The spanwise integration for the force-integration method was calculated using the trapezoidal rule.

Figure 16 shows the moments due to the individual forces: aerodynamic, inertial, and centrifugal. Figure 17 shows the BRAL state-vector moment; curvature-method moment; force-integration moment, 100 intervals; and the force-integration moment, 300 intervals. Although the step size is variable in the BRAL analysis, force-integration moments calculated from the BRAL state vector and in CAMRAD use uniformly spaced intervals. The results seen in Fig. 17 are very similar to those from the CAMRAD/force-integration and CAMRAD/curvature methods. The force-integration moments with 100 intervals accumulates error toward the blade root, and the curvature method is in error in the region of rapidly changing stiffness.

The force-integration results with 100 and 300 intervals show that an insufficient number of spanwise integration steps can result in the kind of error seen in the CAMRAD/force-integration results. This indicated that a realistic rotor such as the CH-34 requires at least 300 spanwise intervals using this implementation of the force-integration method. It also indicates that the integration scheme is critical whereas numerical problems associated with the difference of large numbers do not cause problems in this calculation.

Figures 16 and 17 taken together illustrate another possible source of error for the force-integration method. Near the blade root, the magnitude of the total structural moment is less than 1% of the largest moment component. Therefore, a small error in the calculation of aerodynamic, inertial, or centrifugal moments may give rise to a large error in the structural moment.

Additional insight may be gained by considering the individual forces calculated with the force-integration method. Figure 18 shows the individual component forces, and Fig. 19 shows the sum of the component forces compared with the BRAL state-vector shear force. The components of the shear force and the sum of shear forces were computed at 100 intervals along the blade. Agreement between the sum of the component forces and the state-vector shear force is very good. This indicates that fewer intervals are needed to accurately calculate shear forces than are needed for bending moments.

Figure 20 demonstrates the agreement between shear-force calculations of BRAL and CAMRAD. The agreement of shear forces is very similar to the agreement seen in the deflected shapes in Fig. 8. This is not surprising since the airloads are identical for the two analyses and the inertial forces are calculated from the deflected shapes.

CONCLUSIONS

The isolated problem of calculating flapwise bending moments from a known aeroelastic equilibrium solution has been explored. A comprehensive rotorcraft analysis, CAMRAD, was used to obtain this solution and to demonstrate the force-integration and curvature methods of calculating bending moments. A finite-difference method, BRAL, was used to obtain accurate flapwise bending moments. These were compared with calculations using the force-integration and curvature methods to make general conclusions about the two methods.

It was concluded that the CAMRAD/force-integration method accumulates error as the moment is integrated from tip to root. The CAMRAD/curvature method gives results that are good or bad depending on the radial station. Radial stations away from rapid changes in stiffness were shown to give excellent results; results near these rapid stiffness changes must be ignored. The CAMRAD shear forces, which are the integrated aerodynamic and inertial forces, showed no accumulation of error toward the blade root. These results are general to the extent that they are caused by the complex structure of existing full-scale rotors. That

is not to say that these problems cannot be overcome by another implementation with sufficient degrees of freedom or by a more sophisticated integration scheme. In fact, when applied to the BRAL solution, the force-integration method was shown to give accurate bending-moment results, provided there were enough integration steps.

APPENDIX: DESCRIPTION OF ROTORS ANALYZED

The structural responses of three rotor systems, the CH-34, SA349/2, and BO-105, were calculated and compared with test results. The source of the structural properties, test data, and a description of difficulties encountered in modeling these rotors follows.

The structural properties for the CH-34 rotor were taken from Ref. 15. Calculated airloads and bending moments were compared with test data from the wind-tunnel test described in Ref. 13. Bending moments were converted from blade stresses,[15] using the stress-moduli value reported in Ref. 15. The CH-34 rotor, with coincident flap and lag hinges and blade designed to minimize flap/lag/torsion couplings, was easily modeled by both CAMRAD and BRAL. The wind-tunnel test, however, had a split tip-path plane because of the swashplate actuator installation. This was not modeled by the analyses, which assume identical blades.

The structural properties, airloads, and bending moments for the SA349/2 rotor were all taken from the flight test reported in Ref. 16. Static values of the flap-bending moment were not used in comparisons, a result of calibration problems. The CAMRAD model of the SA349/2 hinge arrangement is only approximated. The hinge sequence is flap/feather/lag from inboard to outboard; therefore, as the blade feathers, the axis of the lag hinge changes relative to the fixed axis of the flap hinge. CAMRAD, however, requires that the flap and lag hinge axes be perpendicular to one another. The CAMRAD and BRAL results shown here model the flap hinge accurately, but the lag hinge remains fixed regardless of pitch input.

The structural properties of the BO-105 are available in Refs. 17 and 18. Bending moments were taken from the flight test of Ref. 17. Airloads have not been measured; therefore, no test data are compared with CAMRAD predictions. Cantilever root end boundary conditions are used to model this hingeless rotor.

Rotor parameters of interest are listed in Table 1. Shown in Fig. 14 are the flapwise stiffness and mass distributions for these rotors. All three rotors have a build up of structure near the root end of the blade seen as an increase in stiffness and mass. Additionally the SA349/2 has several changes in stiffness and mass near the blade tip, and the CH-34 has small changes in mass distribution owing to instrumentation and tip weights.

ACKNOWLEDGMENTS

For their SA349/2 CAMRAD input files and time spent explaining CAMRAD results, I would like to thank Ruth Hefferman, Wayne Johnson, and Gloria Yamauchi. Also, for his BO-105 CAMRAD input files, the help of Randy Peterson is acknowledged.

REFERENCES

[1] Johnson, W., *Helicopter Theory*, Princeton, N.J.: Princeton University Press, 1980.

[2] Curtiss, H. C., Jr. and Shupe, N. K., "A Stability and Control Theory for Hingeless Rotors," Paper No. 541, American Helicopter Society 27th Annual National Forum, May 1971.

[3] Bielawa, Richard L., "Blade Stress Calculation—Mode Deflection vs. Force Integration," *Journal of the American Helicopter Society*, Vol. 23 (3), July 1978, pp. 10-16.

[4] Hodges, Dewey H., "Vibration and Response of Nonuniform Rotating Beams with Discontinuities," *Journal of the American Helicopter Society*, Vol. 24 (5), Oct. 1979, pp. 43-50.

[5] Yamauchi, G. K., Hefferman, R. M., and Gaubert, M., "Correlation of SA349/2 Helicopter Flight Test Data with a Comprehensive Rotorcraft Model," Paper No. 74, Twelfth European Rotorcraft Forum, Sept. 1986.

[6] Hefferman, Ruth M., "Effect of Helicopter Blade Dynamics on Blade Aerodynamics and Structural Loads," AIAA Dynamics Specialists Conference, April 1987.

[7] Callahan, C. and Bassett D., "Application of a Comprehensive Analytical Model of Rotorcraft Aerodynamics and Dynamics (CAMRAD) to the McDonnell Douglas AH-64A Helicopter," American Helicopter Society 43rd Annual National Forum, May 1987.

[8] Johnson, W., "A Comprehensive Analytical Model of Rotorcraft Aerodynamic and Dynamics, Part I: Analysis Development," NASA TM-81182, 1980.

[9] Houbolt, J. C., and Brooks, G. W., "Differential Equations of Motion for Combined Flapwise Bending, Chordwise Bending, and Torsion of Twisted Nonuniform Rotor Blades," NACA Report 1346, 1958.

[10] Johnson, W., "Wake Model for Helicopter Rotor in High Speed Flight," NASA CR-177507, 1988.

[11] Johnson, W., "CAMRAD/JA; A Comprehensive Analytical Model of Rotorcraft Aerodynamic and Dynamics; Johnson Aeronautics Version; Volume I, Theory Manual," Johnson Aeronautics, Palo Alto, Calif., 1988.

[12] Esculier, J. and Bousman, W. G., "Calculated and Measured Blade Structural Response on a Full-Scale Rotor," American Helicopter Society 42nd Annual National Forum, June 1986, pp. 81-110.

[13] Rabbott, J. P., Jr., Lizak, A. A., and Paglino, V. M., "A Presentation of Measured and Calculated Full-Scale Rotor Blade Aerodynamic and Structural Loads," USAAVLABS TR 66-31, July 1966.

[14] Murthy, V. R., "Dynamic Characteristics of Rotor Blades," *Journal of Sound and Vibration*, Vol. 49 (4), Dec. 1976, pp. 483-500.

[15] Neibanck, Charles F., "Model Rotor Test Data for Verification of Blade Response and Rotor Performance Calculations," USAAMRDL-TR-74-29, May 1974.

[16] Hefferman, R. M. and Gaubert, M., "Structural and Aerodynamic Loads and Performance Measurements of an SA349/2 Helicopter with an Advanced Geometry Rotor," NASA TM-88370, 1986.

[17] Staley, James A., "Validation of Rotorcraft Flight Simulation Program Through Correlation with Flight Data for Soft-in-plane Hingeless Rotors," USAAMRDL-TR-75-50, Jan. 1976.

[18] Dixon, P. G. C., "Design, Development, and Flight Demonstration of the Loads and Stability Characteristics of a Bearingless Main Rotor," USAAVRADCOM-TR-80-D-3, 1980.

Table 1 Rotor parameters.

Item	CH-54	SA349/2	BO-105
Number of blades	4	3	4
Rotor radius, m (in.)	8.53 (336.00)	5.25 (206.85)	4.91 (193.32)
Rotor speed, rpm (rad/sec)	221.68 (23.214)	387.00 (40.526)	425.00 (44.506)
Blade chord, m (in.)	0.416 (16.40)	0.350 (13.80)	0.270 (10.64)
Solidity	0.06220	0.06366	0.07010
Flap hinge offset, e_β/R	0.03571	0.02095	–
Feathering hinge offset, e_θ/R	0.08000	0.04762	0.03500
Lag hinge offset, e_ζ/R	0.03571	0.09048	–
Blade cutout, r/R	0.1500	0.2486	0.1000
Precone, deg	0.0	0.0	2.5

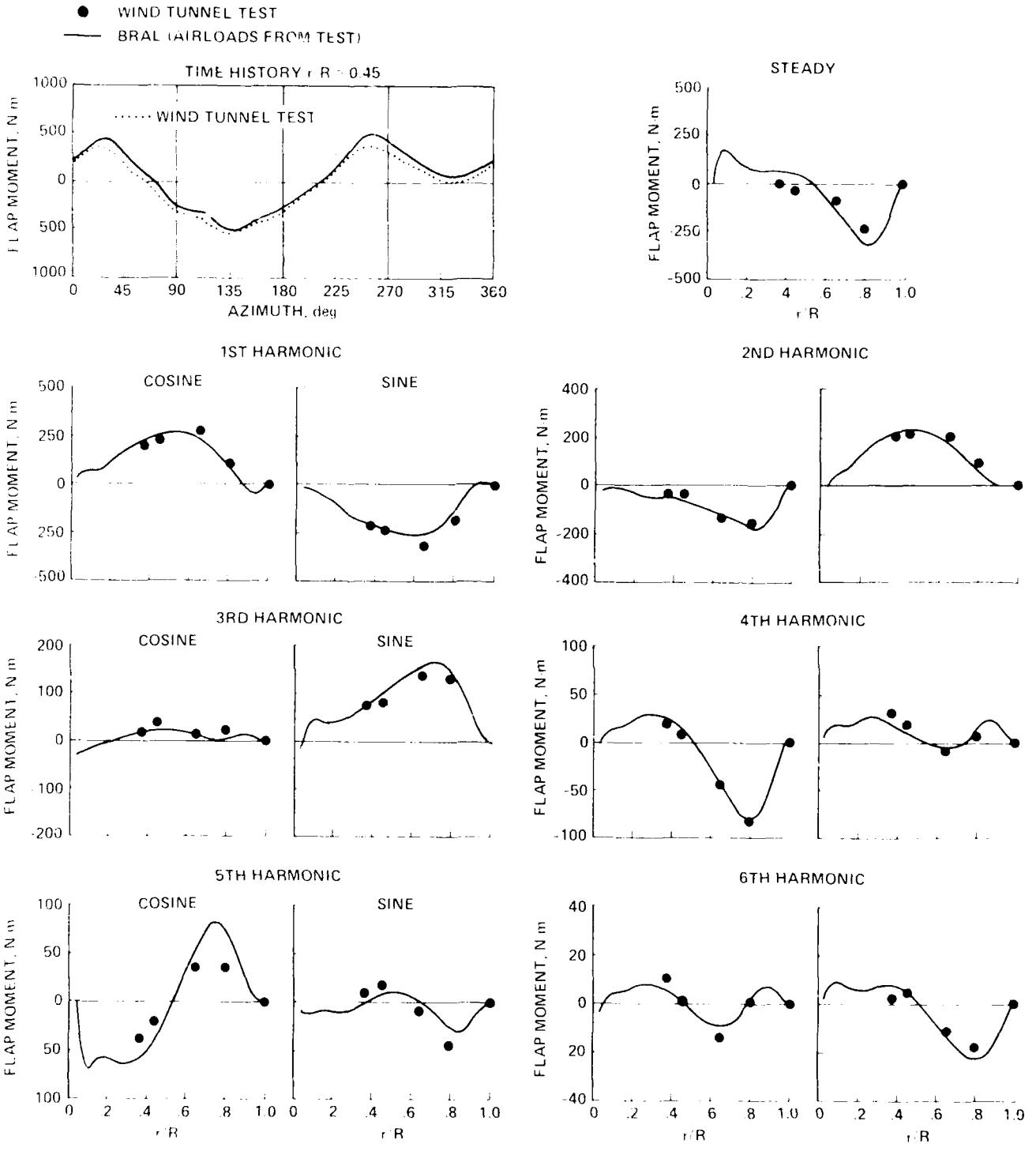

Fig. 1 Comparison of flapwise bending moments, CH-34 rotor: $\mu = 0.39$, shaft angle = -5°.

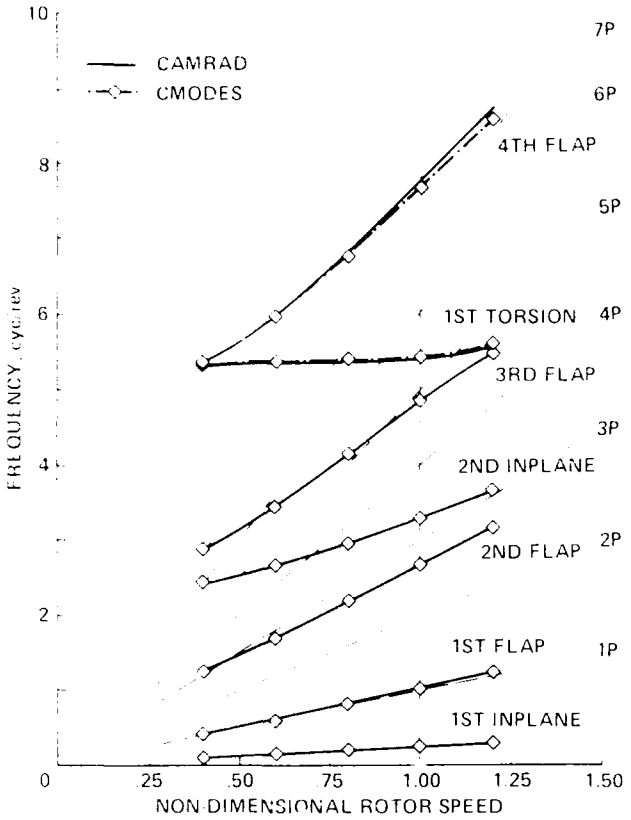

Fig. 2 CH-34 rotor frequency diagram: Ω_0 = 221.7 rpm, $\theta_{3/4}$ = 8.7°.

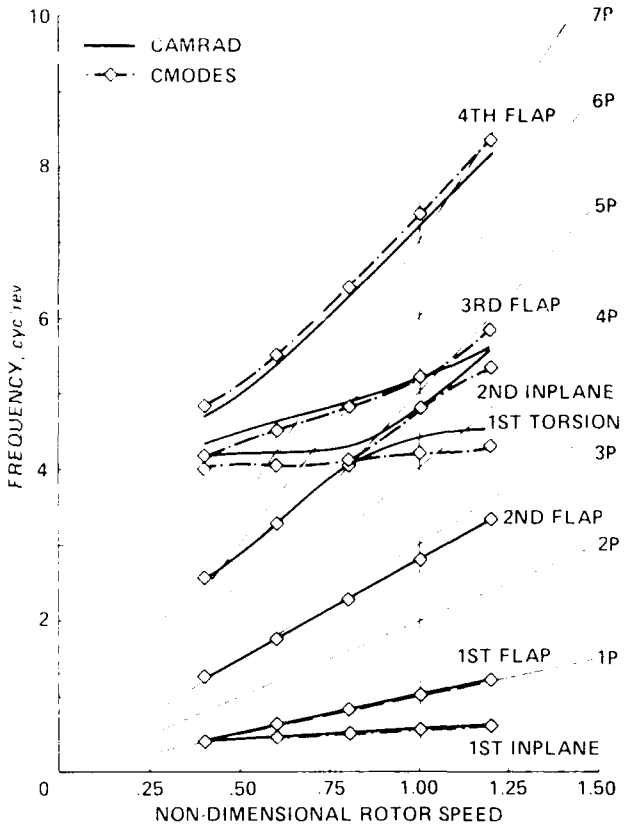

Fig. 3 SA349/2 rotor frequency diagram: Ω_0 = 387.0 rpm, $\theta_{3/4}$ = 10.3°.

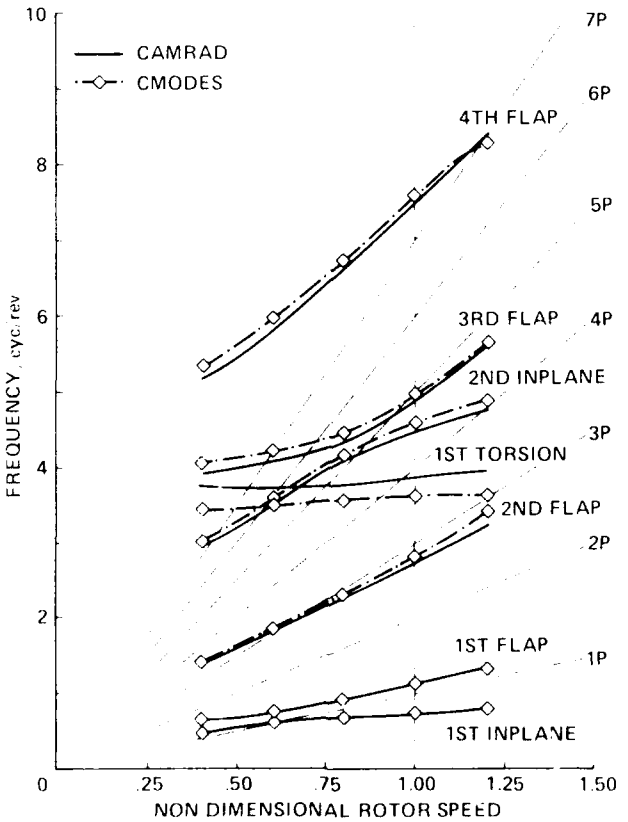

Fig. 4 BO-105 rotor frequency diagram: Ω_0 = 425.0 rpm, $\theta_{3/4}$ = 11.0°.

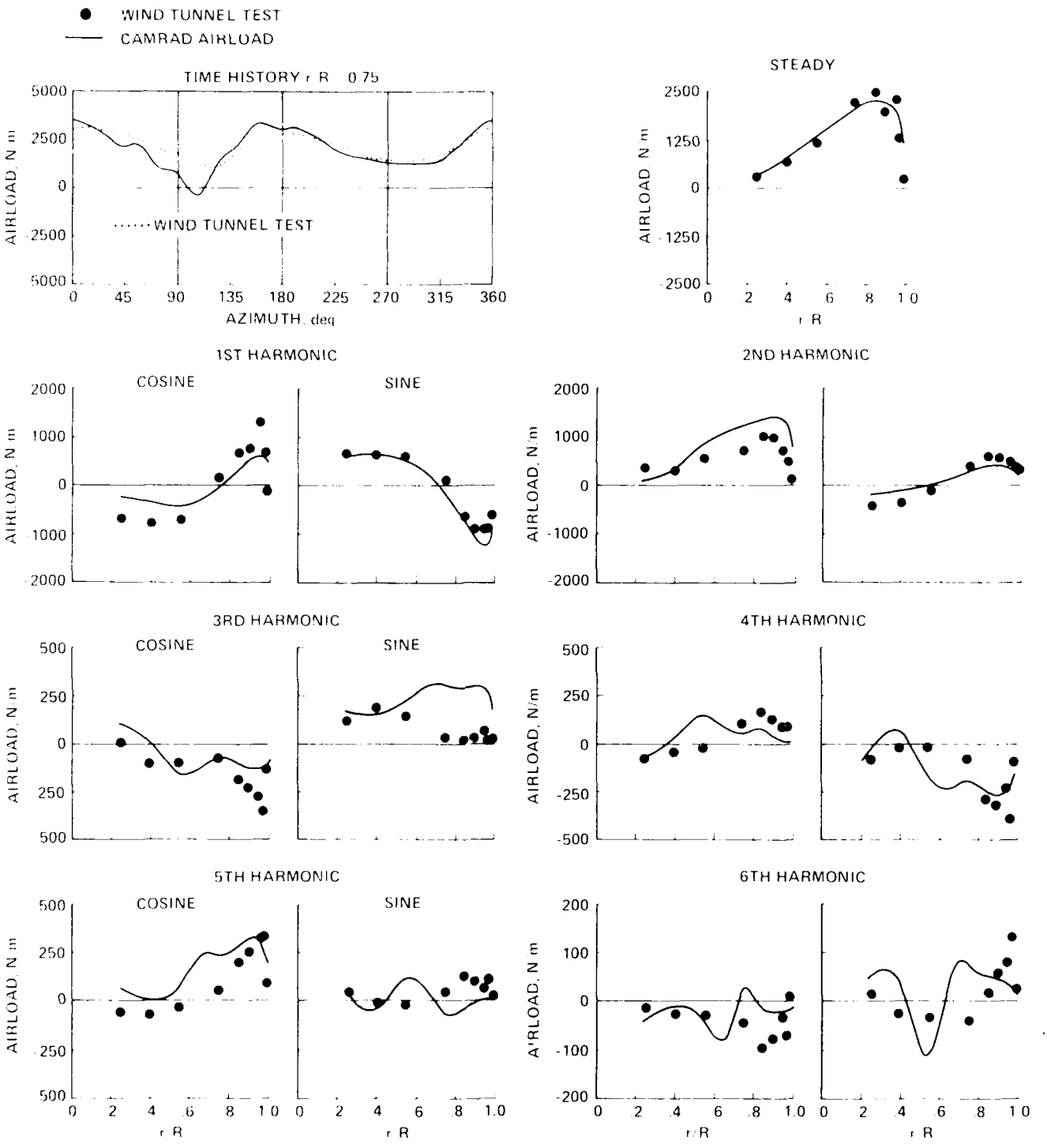

Fig. 5 Comparison of normal airloads, CH-34 rotor: $\mu = 0.39$, shaft angle = -5°.

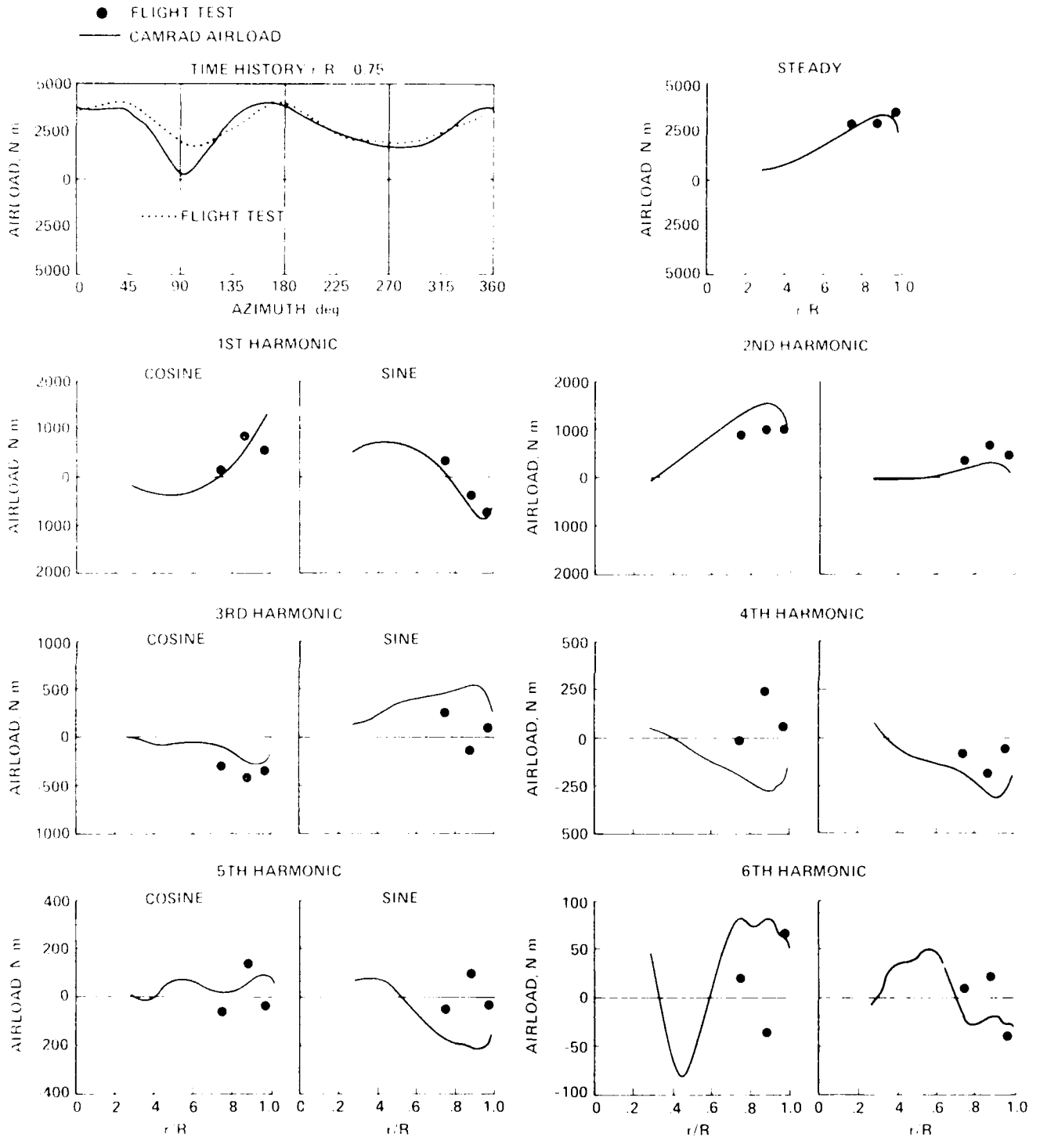

Fig. 6 Comparison of normal airloads, SA349/2 rotor: $\mu = 0.378$, shaft angle = -5.5°.

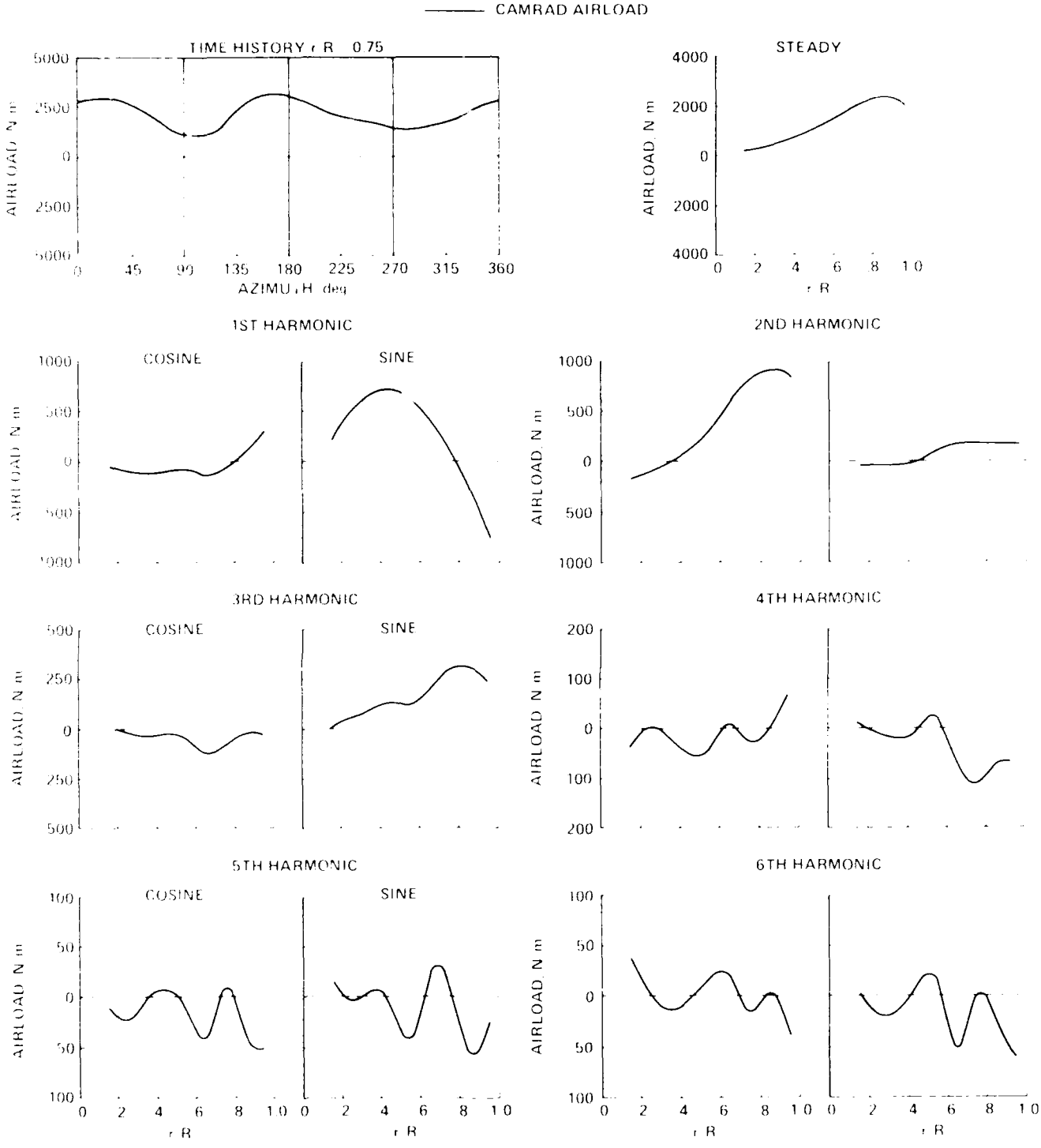

Fig. 7 Normal airloads, BO-105 rotor: $\mu = 0.278$, shaft angle = -5°.

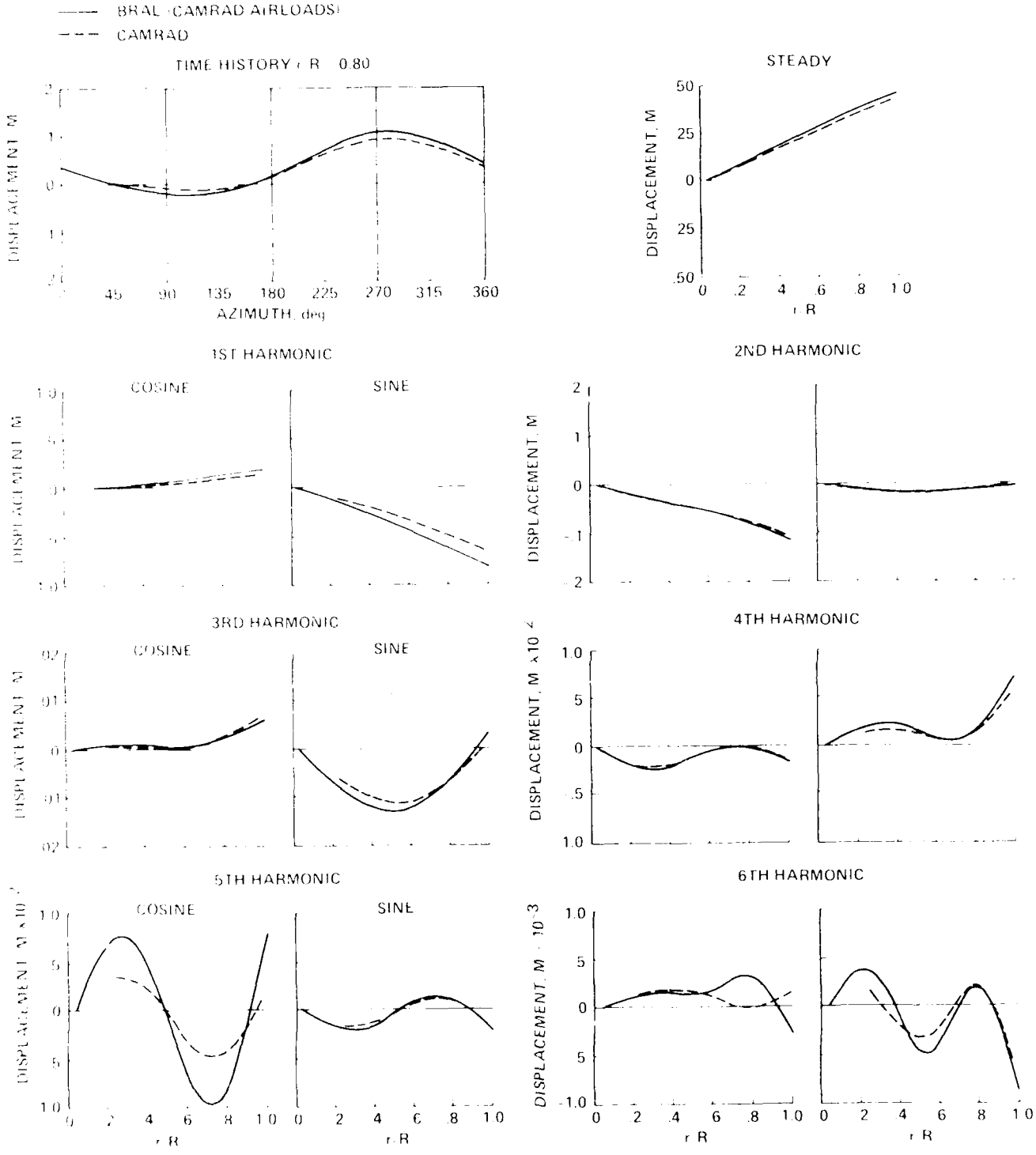

Fig. 8 Comparison of flapwise deflected shapes, CH-34 rotor: $\mu = 0.39$, shaft angle = $-5°$.

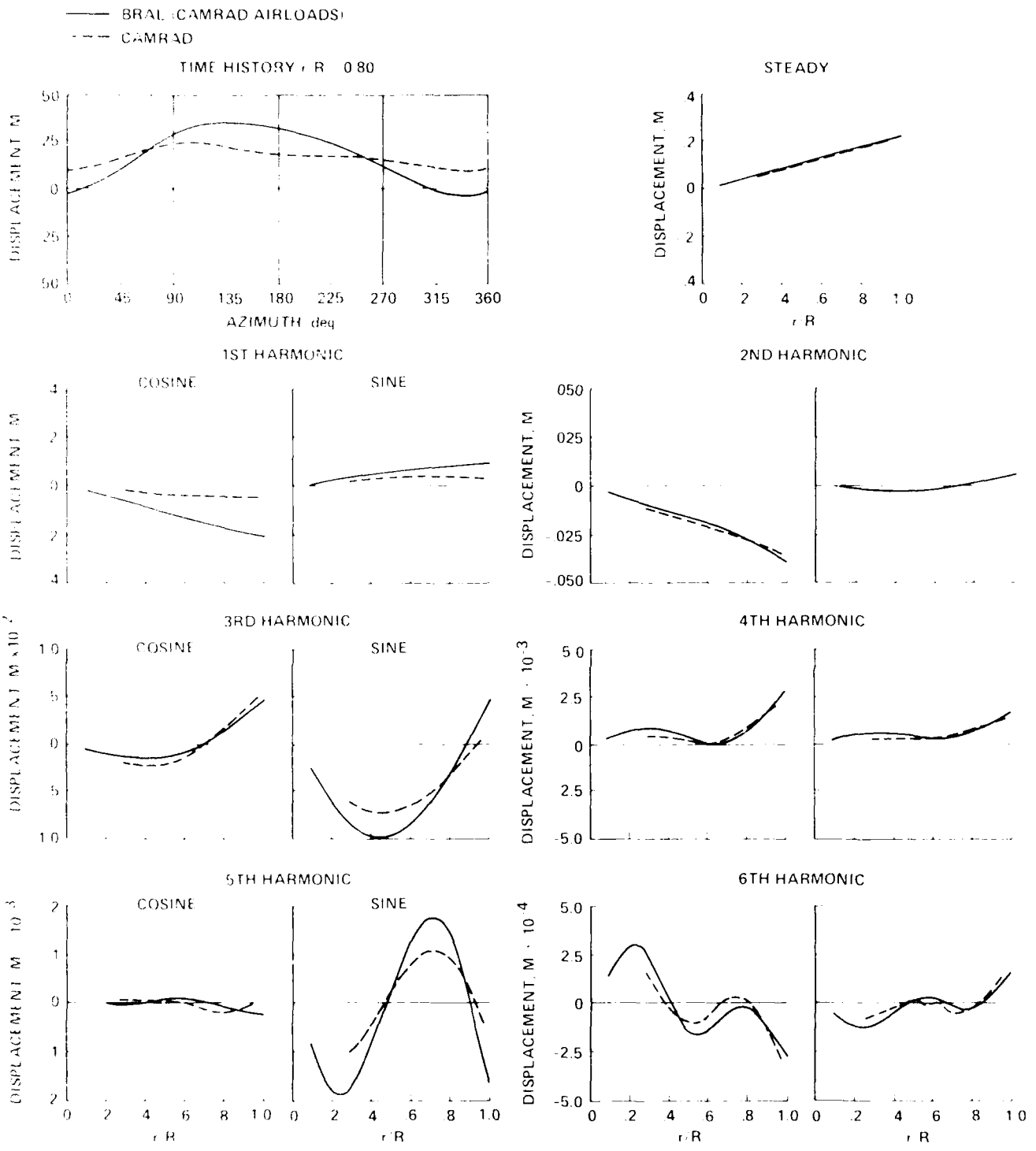

Fig. 9 Comparison of flapwise deflected shapes, SA349/2 rotor: $\mu = 0.378$, shaft angle = -5.5°.

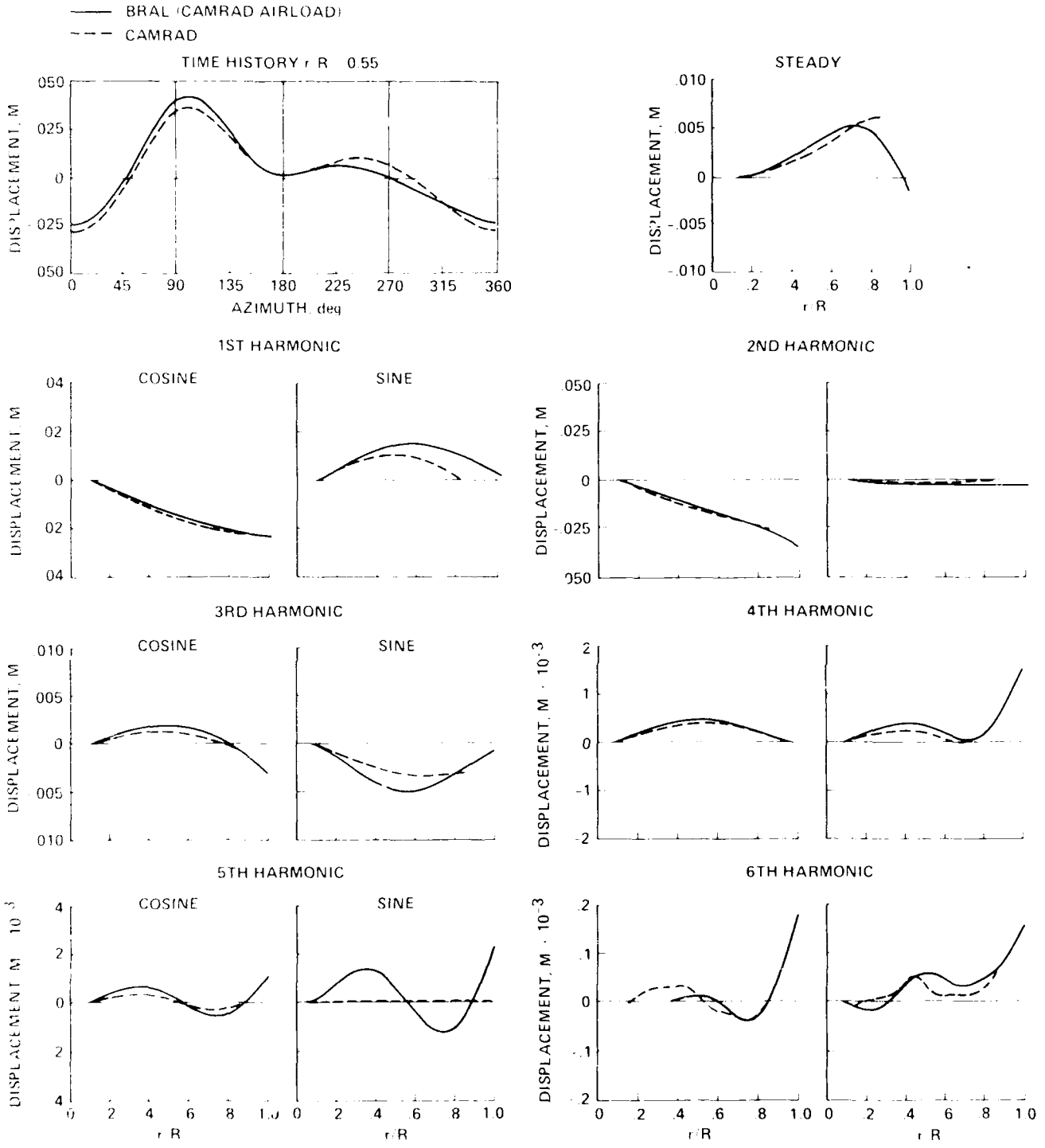

Fig. 10 Comparison of flapwise deflected shapes, BO-105 rotor: $\mu = 0.278$, shaft angle = -5°.

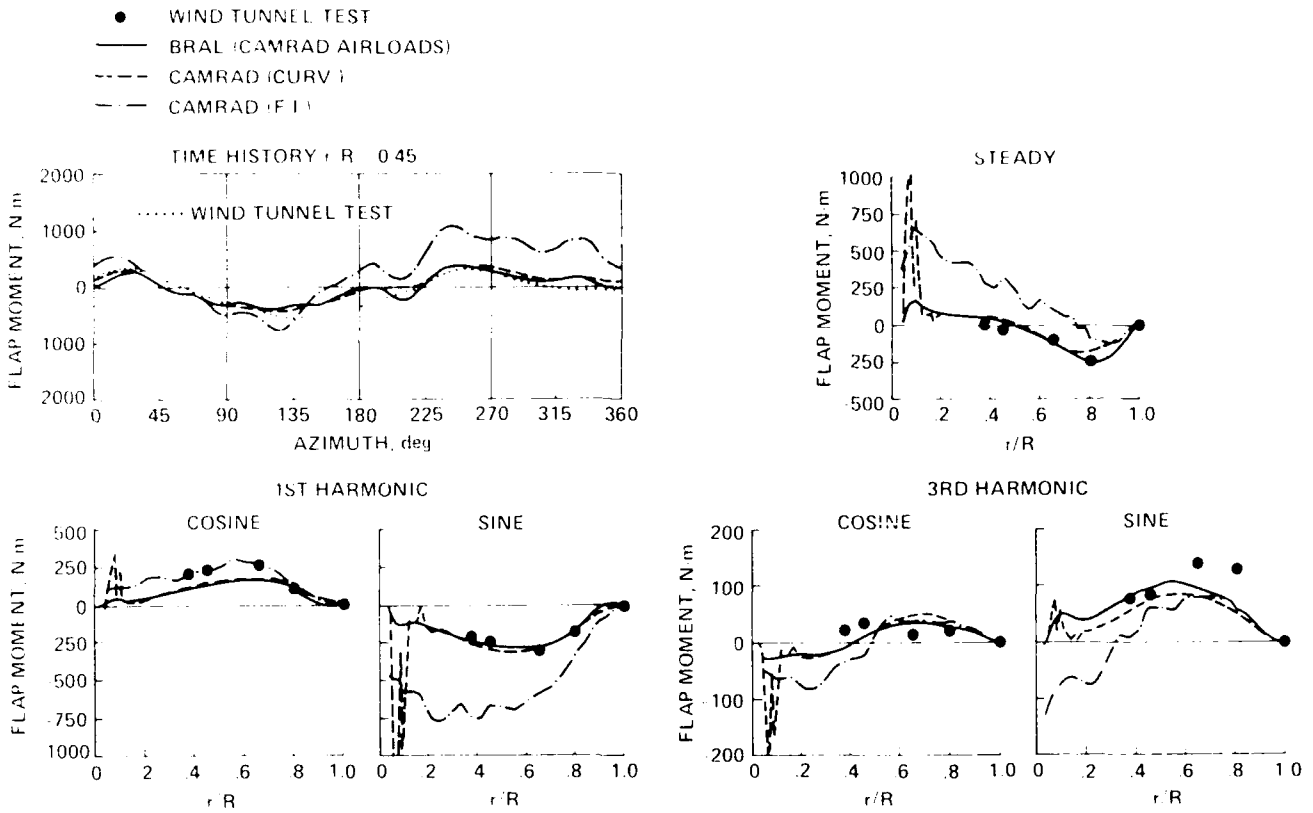

Fig. 11 Comparison of flapwise bending moments, CH-34 rotor: μ = 0.39, shaft angle = -5°.

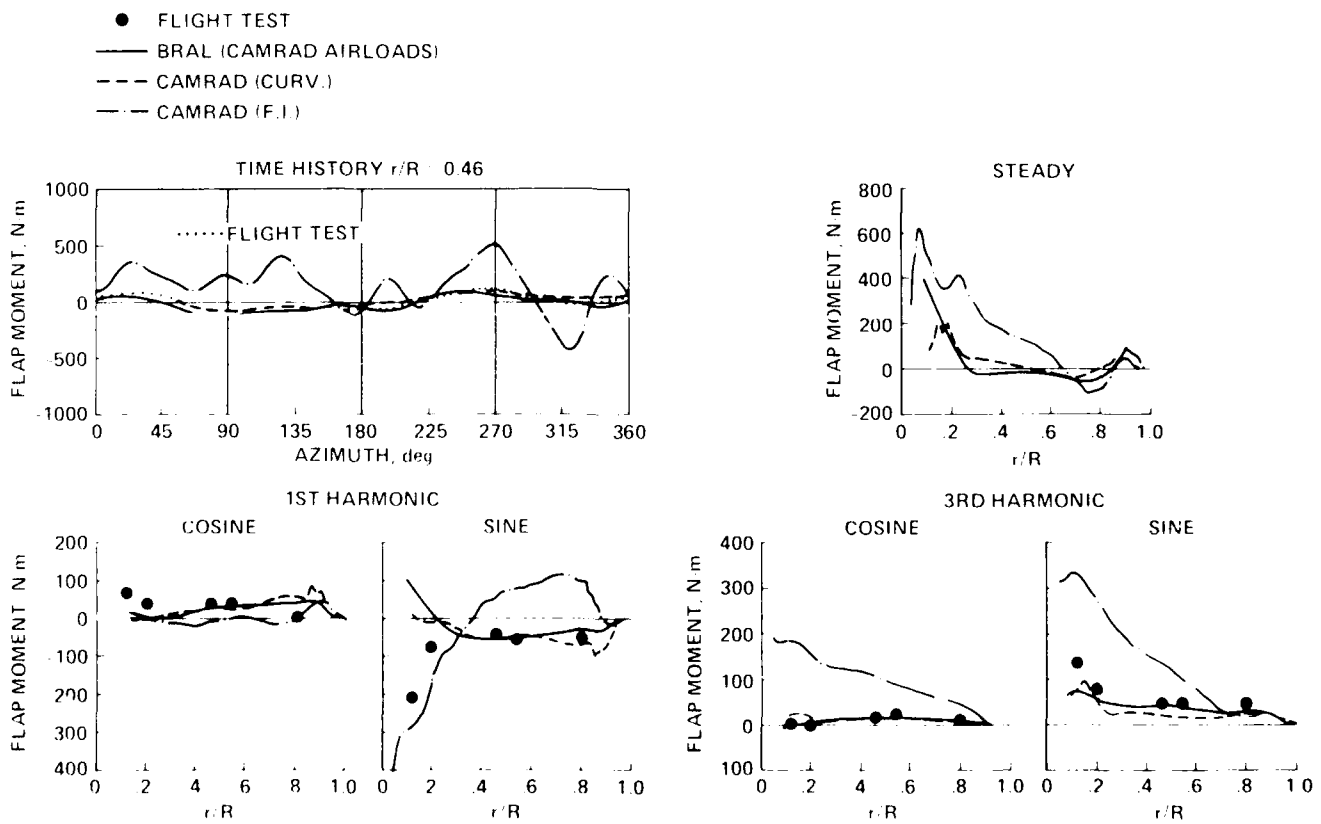

Fig. 12 Comparison of flapwise bending moments, SA349/2 rotor: μ = 0.378, shaft angle = -5.5°.

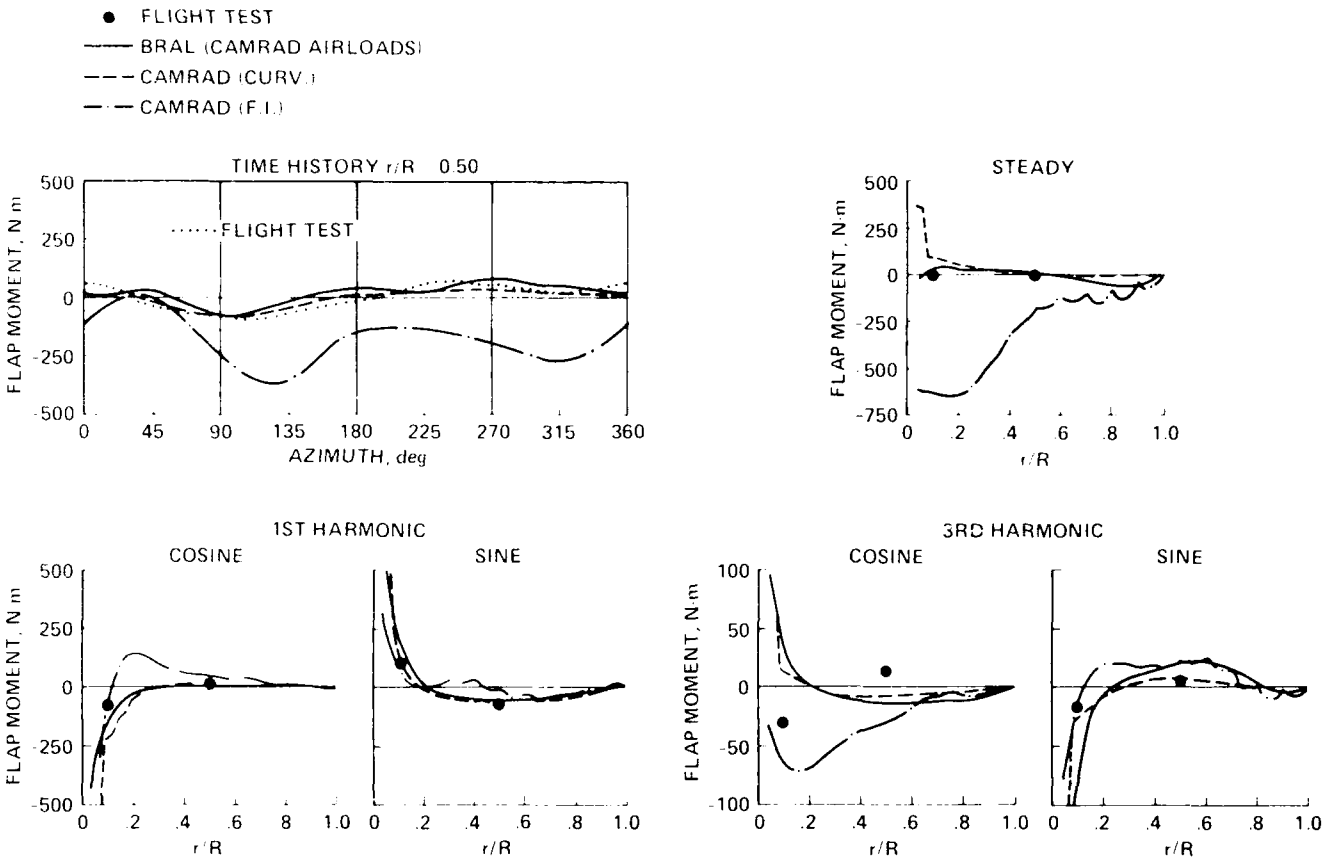

Fig. 13 Comparison of flapwise bending moments, BO-105 rotor: $\mu = 0.278$, shaft angle = -5°.

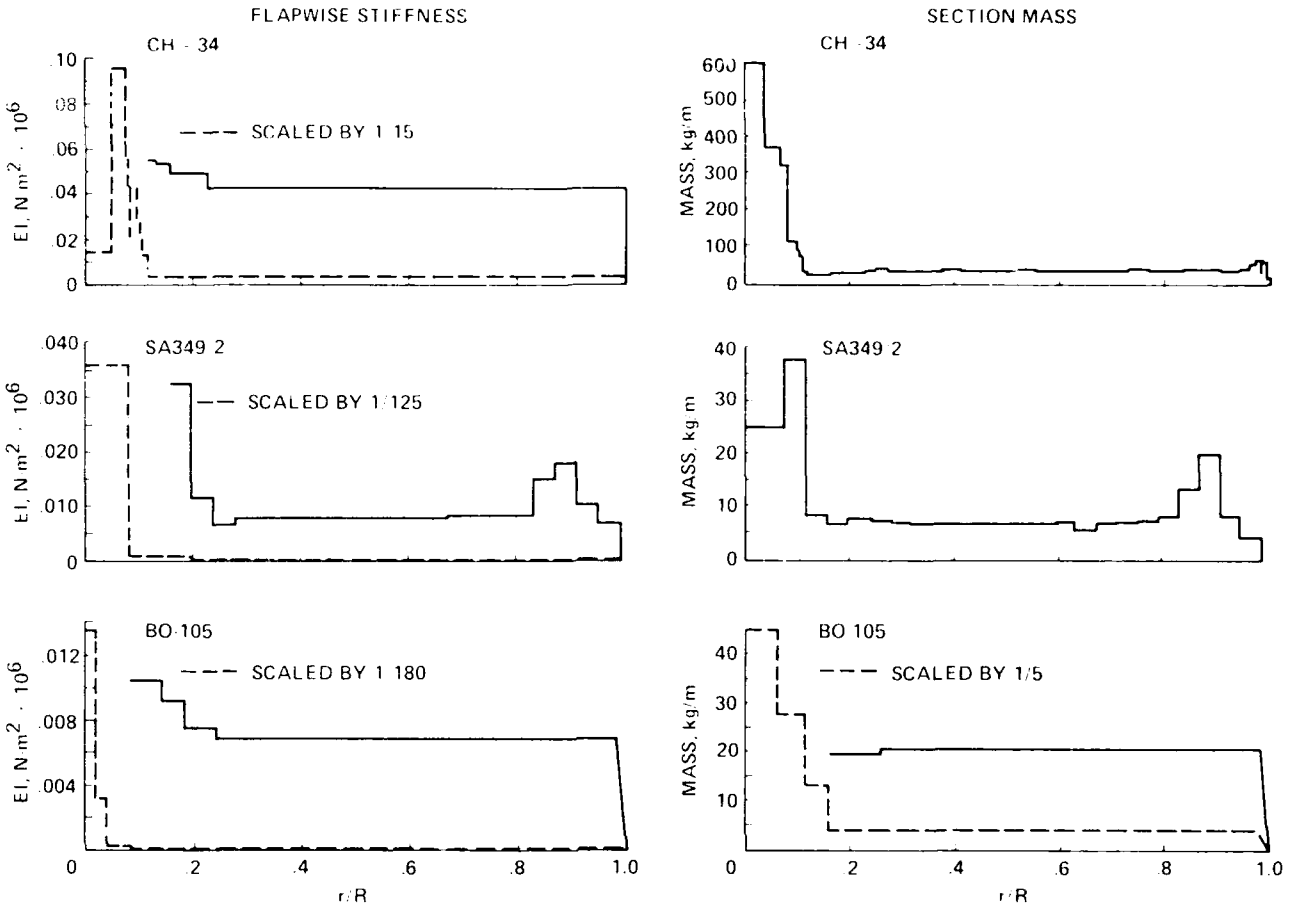

Fig. 14 Flapwise stiffness and mass distribution: CH-34, SA349/2 and BO-105 rotors.

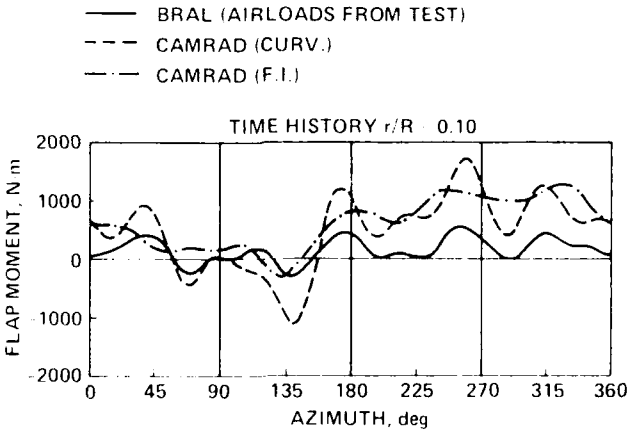

Fig. 15 Example of CAMRAD flapwise moment error, CH-34 rotor: $\mu = 0.39$, shaft angle = -5°.

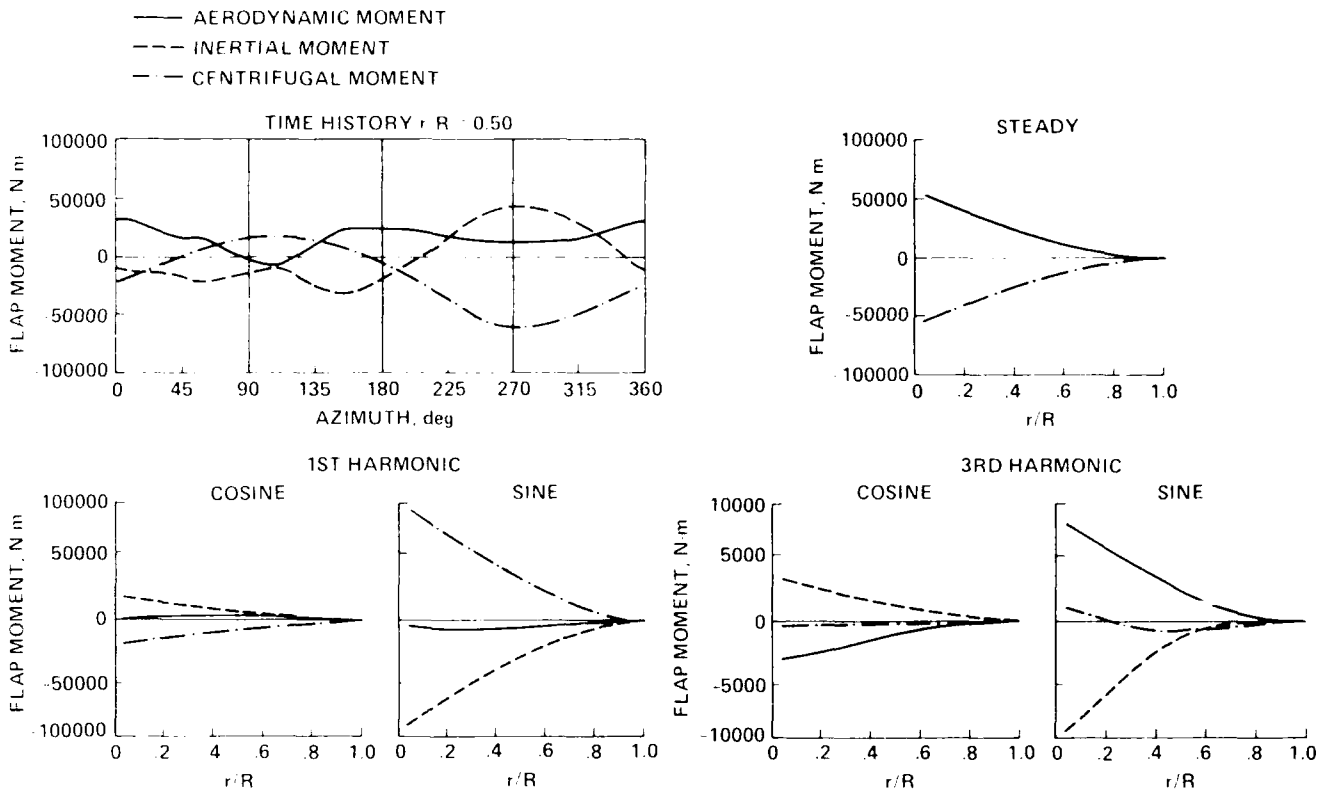

Fig. 16 Components of flapwise bending moment based on BRAL solution, CH-34 rotor: $\mu = 0.39$, shaft angle = -5°.

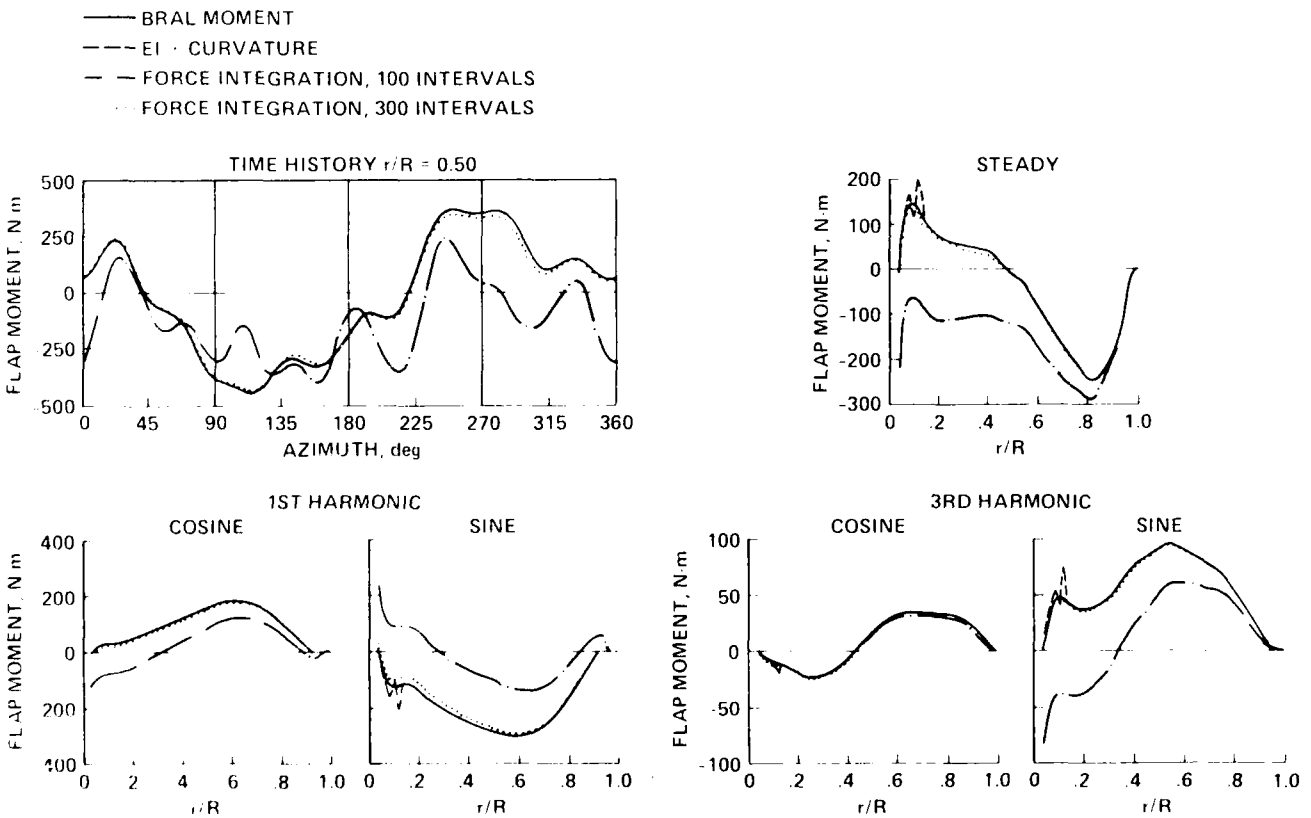

Fig. 17 Comparison of flapwise bending moments, CH-34 rotor: $\mu = 0.39$, shaft angle = -5°.

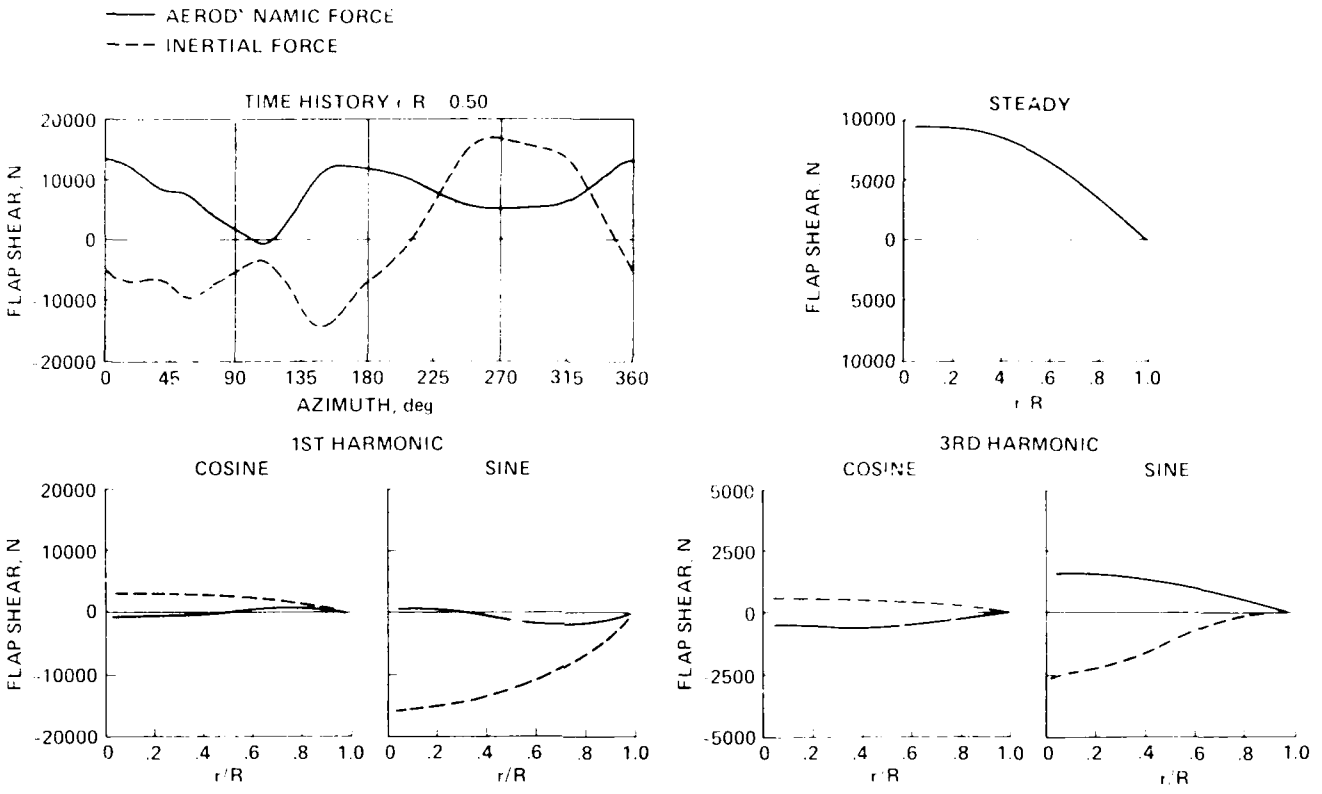

Fig. 18 Components of flapwise shear force based on BRAL solution, CH-34 rotor: $\mu = 0.39$, shaft angle = -5°.

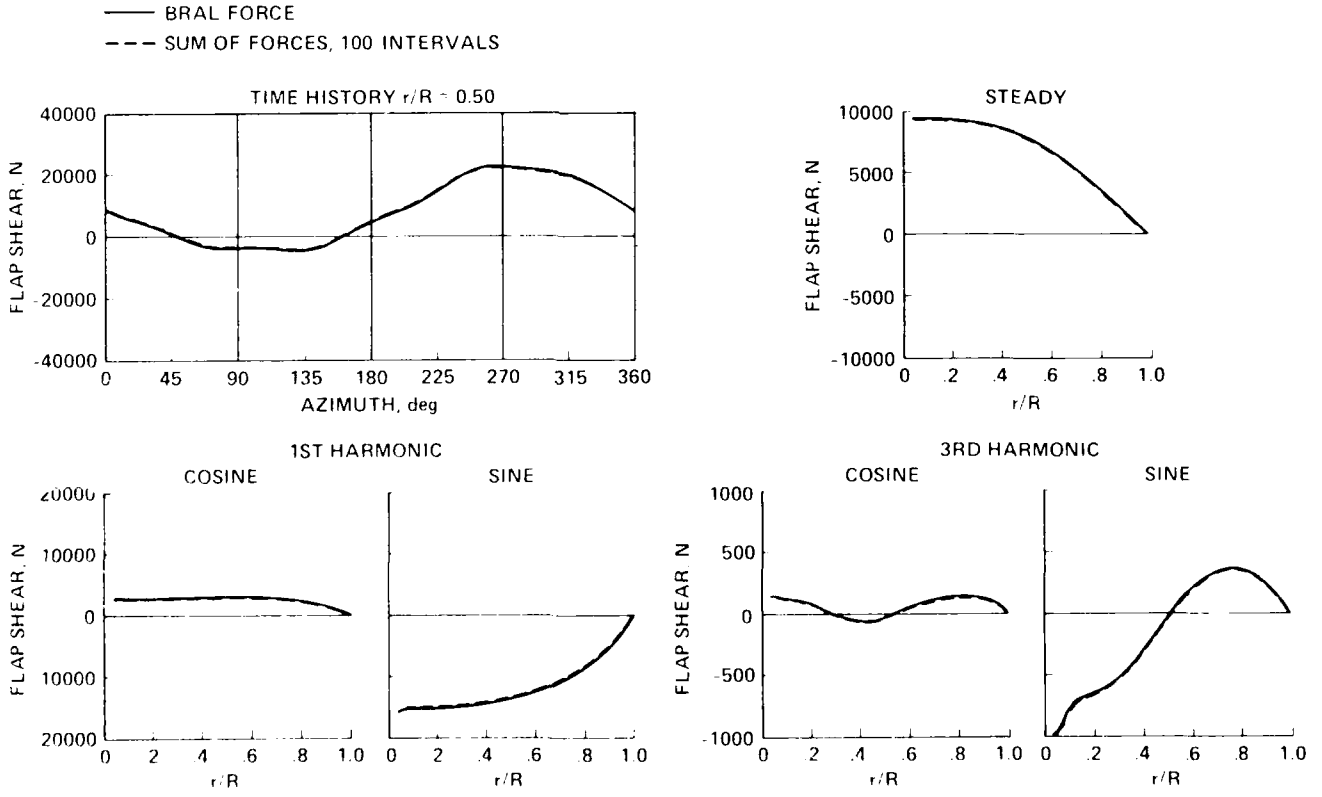

Fig. 19 Comparison of flapwise shear forces, CH-34 rotor: $\mu = 0.39$, shaft angle = -5°.

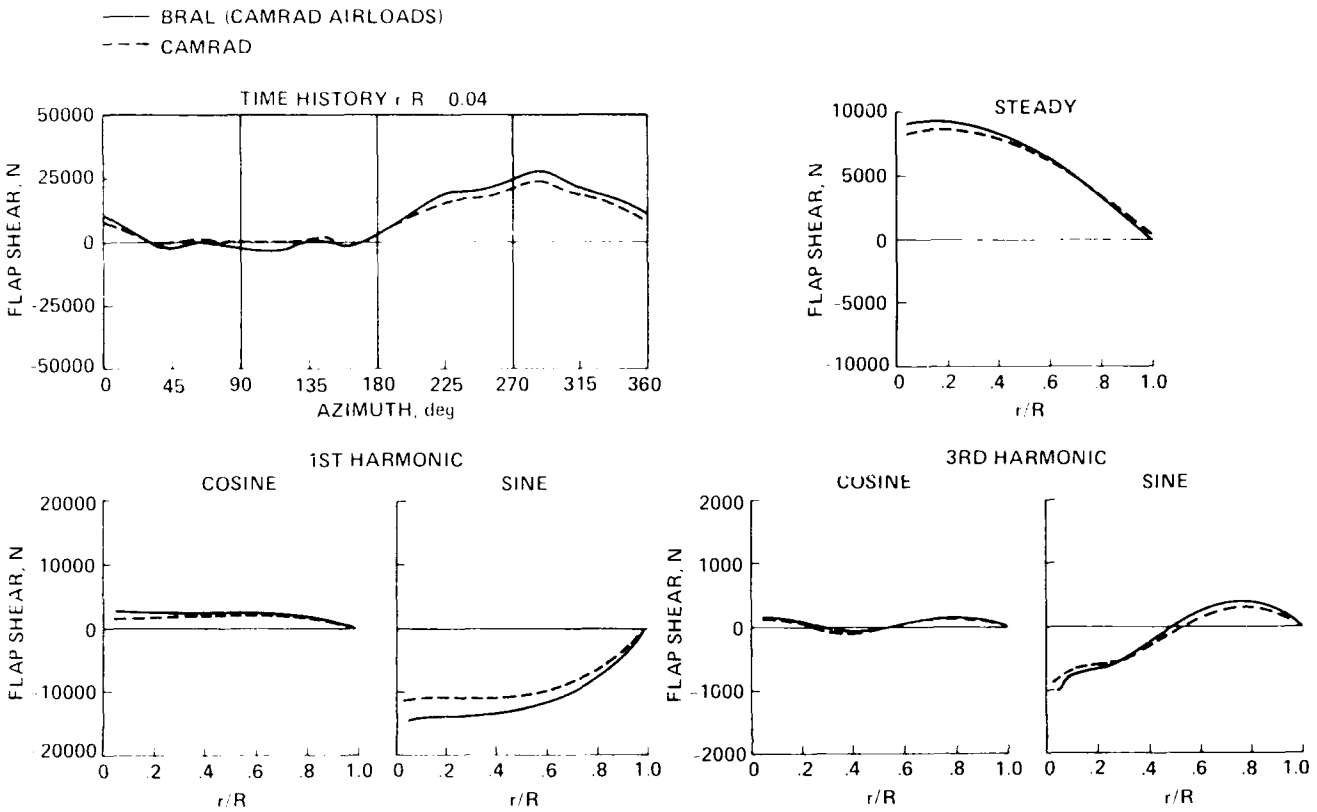

Fig. 20 Comparison of flapwise shear forces, CH-34 rotor: $\mu = 0.39$, shaft angle = -5°.